JOURNAL OF Materials CHEMISTRY

Structural and spectroscopic characterisation of Cr:Li_2MgSiO_4 (γ_0)

Cécile Jousseaume,[a] Andrée Kahn-Harari,*[a] Daniel Vivien,[a] Jacqueline Derouet,[a] François Ribot[b] and Françoise Villain[c,d]

[a]*Laboratoire de Chimie Appliquée de l'Etat Solide, CNRS-UMR 7574, E.N.S.C.P., 11 rue P. et M. Curie, 75231 Paris Cédex 05, France. E-mail: kahnari@ext.jussieu.fr*
[b]*Laboratoire de Chimie de la Matière Condensée, CNRS-UMR 7574, U.P.M.C., 4 place Jussieu, 75252 Paris Cédex 05, France*
[c]*Laboratoire de Chimie Inorganique et Matériaux Moléculaires, ESA CNRS 7071, U.P.M.C, 4 place Jussieu, 75252 Paris Cédex 05, France*
[d] *LURE, UMR 130, Université Paris-Sud, 91898 Orsay Cédex, France*

Received 25th July 2001, Accepted 21st February 2002
First published as an Advance Article on the web 28th March 2002

To understand the exceptionally long fluorescence lifetime of fourfold coordinated Cr^{IV} in γ_0 Li_2MgSiO_4 orthosilicate, the structure of this matrix has been refined from neutron diffraction data. Here we also report the crystal growth of Cr:Li_2MgSiO_4 (low temperature form) by a flux method, and the results of EXAFS and optical investigations of chromium in Li_2MgSiO_4 host lattice.

Introduction

Chromium(IV) ions in a tetrahedral environment, as found in single crystals of forsterite Mg_2SiO_4[1–3] and yttrium aluminium garnet $Y_3Al_5O_{12}$ (YAG),[4,5] have found several applications in optics, for example, tunable laser action around 1.2–1.5 μm[1,4] used in optical fiber communications, ultra-short laser pulse generation[6–8] and passive Q-switching of neodymium activated laser operating at around 1 μm.[9] In YAG and forsterite, chromium ions occur in the III and IV valence states, with Cr^{III} in octahedral sites and Cr^{IV} distributed between the tetrahedral and octahedral sites.[10,11] In YAG for instance, it has been suggested that tetrahedral Cr^{IV}, the active species, represents only a small percentage of the total chromium content.

In order to search for new Cr^{IV} activated laser materials, our strategy was to choose crystalline matrices with only tetrahedral sites, in which Cr^{III} could not enter, that is, we expected that all chromium ions would be in fourfold coordination. This has resulted in the discovery of Cr:Li_2MgSiO_4 (LMS),[12] the most striking feature of which is the very long fluorescence lifetime; more than 100 μs at room temperature. This is more than ten times greater than the value usually reported for Cr^{IV} activated compounds.[13]

Previous work[12] was performed on powdered compounds, but the origin of this very long fluorescence lifetime was not determined. In the present study we hope to gain further knowledge about this compound. Neutron and X-ray diffraction characterisation are performed on LMS. Single crystals of Cr:LMS, suitable for spectroscopic investigations (optical, EXAFS) are obtained by the flux method.

Li_2MgSiO_4 exists as two allotropic modifications: the monoclinic one (γ_0) corresponds to the low temperature ($T < 600$ °C) and the orthorhombic one (γ_{II}), to the high temperature form.[14] The space group of γ_0-Li_2MgSiO_4 is $P2_1/n$ (C^5_{2h}, No. 14) and the dimensions of the monoclinic unit cell were determined to be: $a = 6.300(0)$ Å, $b = 10.692(2)$ Å, $c = 4.995(5)$ Å and $\beta = 90.47(1)°$.[15]

No precise LMS structural determination (atomic position) has been reported to our knowledge. The LMS structure, as deduced from isomorphous Li_2ZnSiO_4, and Li_2CoSiO_4 compounds,[16,17] is based only on tetrahedral sites for Si, Mg and for the two types of Li ions (Fig. 1). Therefore, a structural refinement was performed to determine atomic positions and to evaluate the M–O bond lengths for each cation. The knowledge of cation environment is fundamental to evaluate their capacity to be substituted by chromium and then to understand the origin of the specific optical properties of Cr^{IV}: LMS.

Elaboration and characterisation of polycrystalline LMS

Li_2MgSiO_4 was synthesised by solid state reaction of magnesium hydroxycarbonate, lithium carbonate and SiO_2 in the appropriate molar amounts. Chromium is incorporated during the LMS synthesis as Cr^{III} in Cr_2O_3 (2% at. relative to the Si content), since starting materials with Cr^{IV} are scarce and not easy to prepare. Due to the high affinity of Cr^{III} for octahedral sites, associated with its high crystal-field stabilisation energy in such an environment, it should not enter the LMS lattice, which only offers tetrahedral cationic sites.

The mixture was heated at 1150 °C on a platinum foil in air for 48 h. Optical measurements show chromium in three valence states (4, 5 and 6) in LMS. Reduction under Ar–10% H_2 (8 h at 950 °C) allowed the reduction of Cr^{VI} and Cr^{V}.

Diffuse reflectance is the convenient technique to follow the evolution of chromium oxidation states during the elaboration of LMS. Fig. 2 presents spectra obtained before and after the reduction. Before the reduction, the Cr^{IV} absorption transition is observed, as the $^3A_2 \rightarrow {}^3T_1$ (^3F) broad band[10,18] centred at 680 nm (ranging from 550 to 750 nm). After the reducing

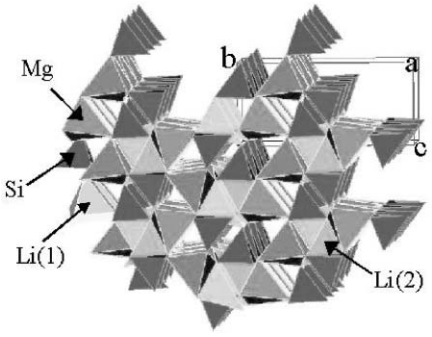

Fig. 1 Structure of monoclinic γ_0 Li_2MgSiO_4.

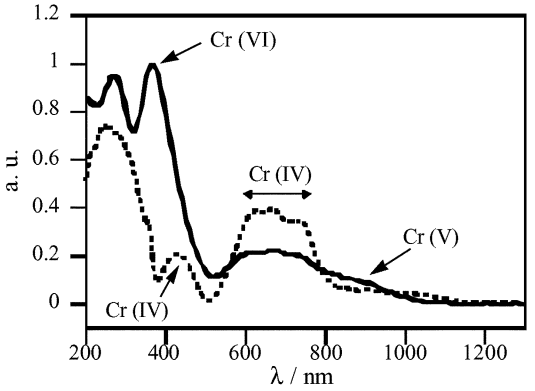

Fig. 2 Diffuse reflectance spectra of Li_2MgSiO_4 before (solid line) and after (dotted line) the reduction under Ar–10%H_2 atmosphere.

treatment, two bands have vanished: one very intense at 370 nm and the second broad band centred at 880 nm. The first absorption peak at 370 nm is attributed to an oxygen-to-Cr^{VI} charge transfer transition.[19] When this peak disappears, it reveals the $^3A_2 \rightarrow {}^3T_1$ (^3P) transition of Cr^{IV} (430 nm). According to data in the literature,[20–22] the second one (centred at 880 nm) can be assigned to Cr^V in a tetrahedral environment, it corresponds to the $^2E \rightarrow {}^2T_2$ transition. The intensity of Cr^{IV} absorption peak (the $^3A_2 \rightarrow {}^3T_1$ (^3F) broad band), is enhanced by the reduction treatment, and this confirms the conversion of tetrahedral Cr^{VI} and Cr^V into Cr^{IV}. The band at 280 nm is observed in both as-prepared and ''reduced'' samples. It may be assigned either to an oxygen-to-Cr^{IV} charge transfer transition, which is expected to occur at lower wavelength than the oxygen-to-Cr^{VI} one, or to the fundamental absorption of the Li_2MgSiO_4 matrix.

For some experiments, carried out with higher chromium content (>10% at. relative to Si content), XRD analysis reveals the presence of a parasitic phase, $LiCrO_2$. This indicates that a limited chromium content can be incorporated into LMS. This second phase, in which Cr^{III} occupies octahedral sites, is also detected by XRD for some ''reduced'' powders (when chromium content is greater than 5% at. relative to Si content). Diffuse reflectance does not indicate the presence of Cr^{III} in these samples, since electrical–dipole transitions are less intense in octahedral symmetry than in tetrahedral symmetry.

These results show that during the reduction, Cr^{VI} and Cr^V are reduced not only into Cr^{IV} in LMS but also to Cr^{III}, which is extracted from LMS to form the parasitic phase $LiCrO_2$.

Structural refinement

Structural refinement was performed, from neutron diffraction data. Data collection was performed on undoped polycrystalline powder, at the LLB facilities of CEA- Saclay. As Mg^{2+}, Si^{4+} and O^{2-} have the same number of electrons (*i.e.* 10) their diffusion factors are very close to each other in X-ray diffraction and this would prevent their identification. With neutron diffraction scattering lengths b of atoms have different values ($b_{(Mg)} = 0.5375$, $b_{(Li)} = -0.19$, $b_{(Si)} = 0.415$ and $b_{(O)} = 0.58$).[23]

Conditions for data collection and results of the refinement by the Rietveld method are listed in Tables 1 and 2 respectively. A comparison between the patterns of neutron diffraction with the calculated values is represented in Fig. 3.

Based on these atomic coordinates, bond lengths (M–O) deduced for each cation (Si, Mg, Li(1) and Li(2)), are listed in Table 3.

As seen in Table 3, none of the cations exhibits a regular tetrahedral environment: the range of variations of bond lengths and angles depends on the cation. The silicon site is the least distorted and the smallest, the two lithium sites are the

Table 1 Refinement of γ_0-Li_2MgSiO_4 structure

Crystal structure	Monoclinic
Space Group	$P2_1/n$
Refined lattice constants	
a/Å	6.300(0)
b/Å	10.692(2)
c/Å	4.995(5)
β/°	90.47(1)
Z	4
Neutron wavelength	2.3433 Å
Angular range	$3° < 2\theta < 171°$
Step/(2θ)	0.01°
Reflections number	220
Independent atoms number	8
Structure parameters number	32
Profile parameters number	8
μR_{eff}	0.5
R_B (%)	0.04
R_F (%)	0.03
R_P (%)	0.11
R_{wp} (%)	0.11
R_{exp} (%)	0.09
χ_2	1.52

Table 2 Atomic parameters in the refined structure of γ_0 Li_2MgSiO_4 ($P2_1/n$–space group No. 14)

	Atomic parameters			
Atom	x	y	z	B
Li(1)	−0.0050(21)	0.1595(10)	0.3072(21)	0.20(17)
Li(2)	0.2370(19)	0.0740(9)	0.7155(21)	0.31(18)
Mg	0.4967(7)	0.1645(4)	0.3075(8)	0.52(8)
Si	0.2483(9)	0.4131(4)	0.3134(10)	0.46(9)
O(1)	0.2459(6)	0.4087(3)	0.6429(6)	0.45(8)
O(2)	0.2515(6)	0.5578(3)	0.2113(6)	0.54(7)
O(3)	0.0334(5)	0.3411(3)	0.2034(7)	0.33(7)
O(4)	0.4599(5)	0.3397(3)	0.2077(7)	0.45(7)

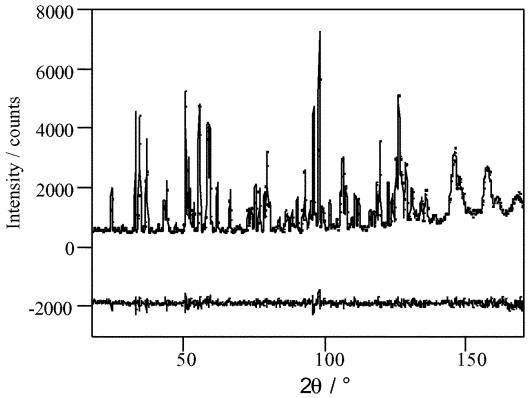

Fig. 3 Rietveld neutron diffraction pattern for Li_2MgSiO_4 (λ = 2.34 Å). Dots correspond to experimental data and lines to the calculated and difference plots.

Table 3 Estimated bond lengths (M–O) for cations of Li_2MgSiO_4 from refined atomic positions/Å

	Si	Mg	Li(1)	Li(2)
Bond lengths/Å				
M–O(1)	1.648(6)	1.943(6)	1.910(12)	1.906(10)
M–O(2)	1.629(5)	1.937(5)	1.935(12)	2.141(11)
M–O(3)	1.648(6)	1.990(5)	2.015(11)	2.077(12)
M–O(4)	1.638(6)	1.951(5)	2.025(11)	1.975(12)
Mean bond length/Å	**1.641**	**1.955**	**1.971**	**2.025**

Table 4 Ionic radii/Å of Li_2MgSiO_4 cations and chromium in various oxidation states[24] (C. N. = coordination number)

	C. N.	Ionic radii/Å
Cr^{III}	6	0.615
Cr^{IV}	4	0.41
Cr^{V}	4	0.345
Cr^{VI}	4	0.26
Li^{I}	4	0.59
Mg^{II}	4	0.57
Si^{IV}	4	0.26

largest and the most distorted. Due to its charge, Cr^{IV} would rather replace silicon in the lattice, but due to its size, it is not so straightforward ($r(Si^{IV})$ = 0.26 Å and $r(Cr^{IV})$ = 0.41 Å Table 4). From a comparison of the ionic radii for chromium (in various oxidation states) and for the cations of LMS in tetrahedral symmetry, no conclusion about the crystallographic location of Cr^{IV} (Table 4) can be deduced. In fact, according to the size criterion, Cr^{IV} could also substitute magnesium.

Crystal growth

The LMS melting (~1470 °C) was reported to be congruent in the phase diagram determined by West.[14] However, due to the high loss of volatile Li_2O, crystal growth of LMS from the melt is not possible. Therefore the convenient technique to obtain crystals is the "flux method".

Single crystals of LMS were grown using the slow cooling flux method, with LiF as solvent. This solvent was chosen because it forms a eutectic with LMS, it does not add an extracation, which could pollute the crystals, it can compensate the loss of lithium at high temperatures and is soluble in hot water.

The crystallisation temperatures of several LiF–LMS mixtures were determined by DTA measurements, in order to establish the LiF–LMS pseudo binary diagram. Starting materials are commercial LiF (99.9%) and LMS powder formerly prepared with initial chromium doping equal to 5% at. (1.94% wt.). Part of the LiF–LMS phase diagram is given in Fig. 4.

From these results, crystal growth was performed with a 30% Cr:LMS–70% LiF mixture, carefully homogenised, in a platinum crucible at 1200 °C and then slowly cooled (2 °C h^{-1}) in the appropriate temperature range (from 1100 to 900 °C). The crystal growth takes place under an air atmosphere. Such obtained crystals are plate-like. The largest ones are a few millimeters sized (10 mm × 7 mm × 2 mm) but they contain LiF inclusions and are of poor crystal quality which makes them unsuitable for single crystal neutron diffraction studies. Nevertheless, X-ray diffraction confirms that these crystals are

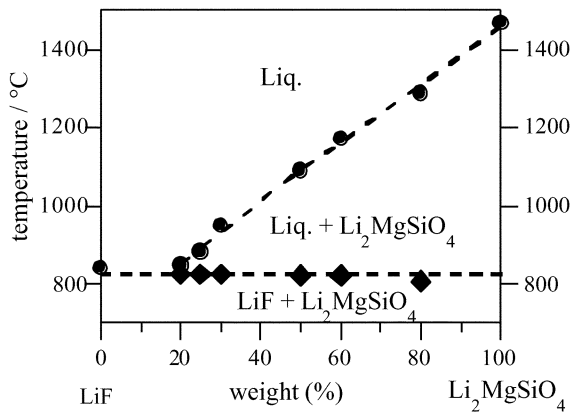

Fig. 4 Partial LiF–Li_2MgSiO_4 phase diagram (weight %) from DTA experiments (Liq. = liquid).

LMS. Preliminary chemical analyses (by X-ray fluorescence and by ICP) indicate that the crystal content is below 0.03% wt. of chromium, taking into account all oxidation states (note the starting materials contain 1.94% wt. of chromium). This demonstrates that the chromium solubility in these crystals is very low. Therefore, its localisation in this lattice cannot be determined by classical X-ray diffraction techniques.

Diffuse reflectance on ground crystals shows the presence of three valence states (IV, V and VI) for chromium, as in the initial powders prepared by solid state reaction. Some experiments were also done with Cr^{IV}:LMS as starting compound, prepared by a reducing treatment of $Cr^{IV, V, VI}$:LMS under Ar–H_2. With Cr^{IV}:LMS the crystal growth was performed either in air or in argon. In air, crystals still contained chromium with the three valence states (IV, V and VI). Under an argon atmosphere, no crystals were obtained. There is no Cr^{VI} when working under an inert atmosphere, crystal growth does not take place. Indeed, Cr^{VI}, which may act as a nucleant agent, appears necessary to grow Cr:LMS crystals.[25]

Fluorescence lifetime in single crystals

Cr^{IV}:LMS fluorescence lifetime was measured on such grown single crystals, under pulsed laser excitation at 760 nm into the $^3A_2 \rightarrow {}^3T_1$ (^3F) transition of Cr^{IV}. This beam was produced by an OPO (optical parametric oscillator) pumped by the third harmonic of a Q-switched Nd:YAG laser (355 nm). The fluorescence was detected with a InGaAs cell and recorded using a sampling oscilloscope (Tektronix TDS 420). The time constant of the measurement was approximately 1 μs.

Fig. 5 presents the fluorescence decay profiles at room temperature and 30 K. It shows that the decays are exponential at both temperatures, and then, interactions between chromium ions are not important in this material. The fluorescence lifetime is 117 μs at room temperature and 305 μs at 30 K. These values are comparable to those already reported for LMS powder samples.[12] This confirms the exceptionally long Cr^{IV} lifetime in LMS and that the $LiCrO_2$ impurity (detected in powder samples but not in single crystals) has no effect on the fluorescence lifetimes.

As the chromium content is less than 0.03% wt., X-ray diffraction techniques are unsuitable to determine the localisation of chromium in the lattice. EXAFS at the chromium K-edge, however, allows the specific study of chromium environment in the LMS structure.

EXAFS local structure investigation

Experimental

X-Ray absorption spectroscopy (XAS) experiments, at the chromium K edge, were performed at LURE, a french synchrotron radiation facility, on the XAS 13 spectrometer (D42 beam line). According to the dilution of chromium in the

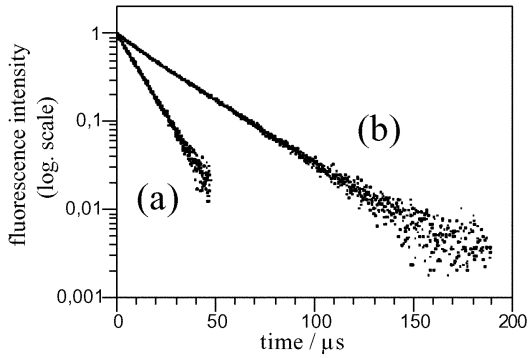

Fig. 5 Cr^{IV}:Li_2MgSiO_4 crystals fluorescence decay profiles recorded at room temperature (a) and at 30 K (b) under excitation at 760 nm.

samples, fluorescence yield spectra were recorded at room temperature using 7 solid state detectors, combined with a multichannel analyzer to select the chromium Kα fluorescence. Two types of samples were studied: Cr:LMS prepared by solid state reaction named "A" and Cr:LMS prepared by the flux method "B".

EXAFS of Cr:LMS (A (powders) and B (ground crystals)) was recorded with a Si111 "channel-cut" monochromator by steps of 4 eV from 5960 to 5980 eV and by steps of 2 eV from 5980 to 6900 eV. Data analysis was performed with the softwares developed by Michalowicz,[26] following standard methods based on single scattering theory.[27,28] The background was computed from the pre-edge region (linear approximation) and subtracted from the spectrum. Atomic absorption was approximated with a fourth degree polynomial. The energy reference for the calculation of the wave vector scale was taken at the absorption maximum (6008 eV). The EXAFS signal was extracted following the Lengeler–Eisenberger formula.[27,28] The Fourier transform of the EXAFS modulations was computed between 1.5 and 11.2 $Å^{-1}$ with a Kaiser truncation window ($\tau = 2.5$).

Results and discussion

The EXAFS investigation provides information on the local environment around chromium (distance to oxygen neighbours), whatever the oxidation states (IV, V and VI).[29]

The first experiments were performed on samples A (2% at. chromium, prepared by solid state reaction) before and after the reduction. Surprisingly, there was no difference between the EXAFS signals of the "reduced" and "air prepared" samples. The comparison of these EXAFS signals and that of pure $LiCrO_2$ (Fig. 6) shows that all powder samples are polluted by this parasitic phase. $LiCrO_2$ was present in all powder samples even at very low chromium content (<2% at.) and even before the reduction. This phase is not detected by XRD for low chromium content (under the detection limit). Nevertheless, $LiCrO_2$ concentrates most of the chromium as Cr^{III}, and its contribution dominates the EXAFS signal of LMS powders. Such results also show that even if chromium is well identified in LMS by diffuse reflectance spectroscopy, its actual solubility into LMS is weak.

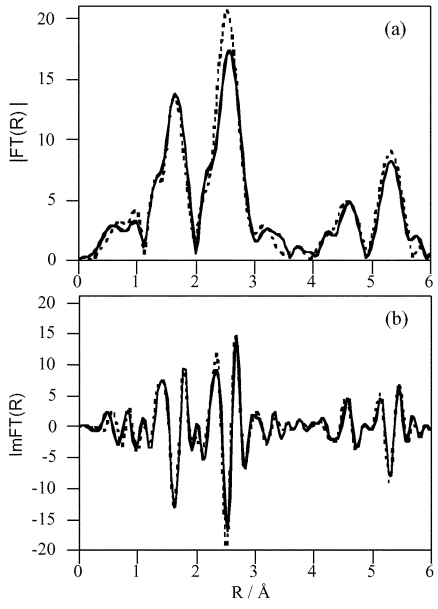

Fig. 6 Comparison between modulus (a) and imaginary parts (b) of Fourier transform Cr K-edge EXAFS signal of "Cr:Li_2MgSiO_4" powder samples, A sample (solid line) and $LiCrO_2$ (dotted line). Chromium signal in "Li_2MgSiO_4" powder is in fact chromium signal in $LiCrO_2$.

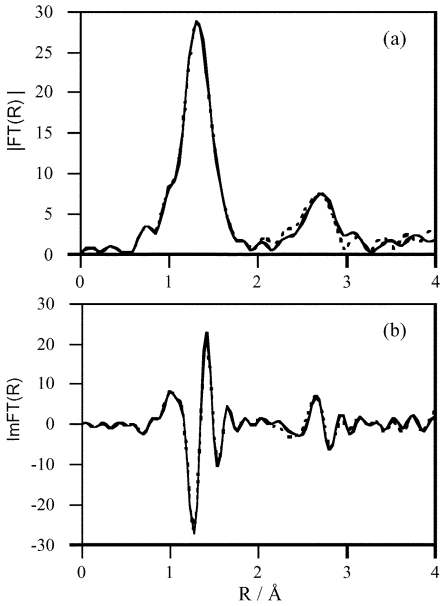

Fig. 7 Comparison between modulus (a) and imaginary parts (b) of Fourier transform Cr K-edge EXAFS theoretical signals of Cr:Li_2MgSiO_4, calculated with single scattering approximation (solid line) and with multiple scattering (dotted line).

In contrast with observations in Cr:LMS powders, EXAFS signal of ground crystals (B sample) should concern only the chromium (4, 5 and 6) inserted into the LMS lattice. Because of the low signal to noise ratio, only the first co-ordination polyhedron of chromium could be analysed. The fitting procedure was performed in the framework of single scattering. Indeed, to check the importance of the multiple scattering, a preliminary study was performed on the theoretical EXAFS signal of chromium set on the silicon site in LMS, using FEFF code (version 7.02).[30–32] The data analysis of the EXAFS signal can be performed with single scattering approximation until 4 Å (Fig. 7). Therefore, the fitting procedure was applied with amplitude, phase shift functions and the mean free path of Cr:Li_2MgSiO_4, from the FEFF code in the framework of single scattering.

To validate the fitting procedure, with amplitude, phase shift functions and mean free path calculated by FEFF, K_2CrO_4, the crystal structure of which is well known, was analysed. The result gives 4.0 oxygen neighbours at a mean distance of 1.67 ± 0.02 Å ($R = 2.1\%$), which is in good agreement with the crystallographic description. The number of neighbours was not fixed during the refinement. Therefore, the amplitude, phase shift functions and mean free path (associated with $S_o^2 = 1$) calculated with FEFF give a significant quantification of the number of neighbours. The result of the fit on Cr:Li_2MgSiO_4 ground crystals (B sample) is given in Fig. 8, which presents (a) the modulus of the experimental Fourier transform of the EXAFS signal and (b) the experimental and fitted EXAFS signal. The best agreement ($R = 1.3\%$) was obtained with two types of chromium environment and a total coordination number of 4.3 oxygen neighbours. The first shell of oxygen ($N = 2.4$) is located at a mean distance of 1.68 ± 0.02 Å, the second one ($N = 1.9$) at a mean distance of 2.07 ± 0.02 Å. The first distance (Cr–O = 1.68 Å) is similar to the one encountered in the silicon environment in LMS (average Si–O bond length = 1.64 Å). It can be compared to Mg_2SiO_4, where Cr^{IV} is supposed to substitute the silicon since Cr^{IV}–O distance found by Miyano *et al.* is 1.68 ± 0.03 Å.[29] The second type of environment (Cr–O = 2.07 Å) corresponds to a larger site which can be compared to those of lithium or magnesium in LMS structure. This distribution could be related to the various oxidation states of chromium. Considering the ionic radii of

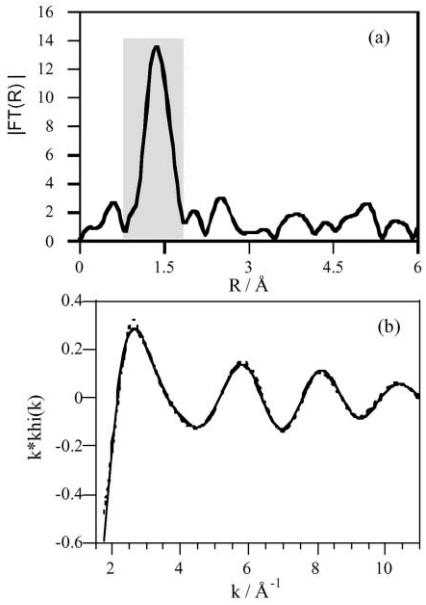

Fig. 8 EXAFS results on Cr:Li_2MgSiO_4 ground crystals, B sample, at the chromium K-edge. (a) Modulus of the experimental Fourier transform of the EXAFS signal and (b) experimental (solid line) and fitted EXAFS signal (dotted line).

Cr^{VI} (Table 4), we can suppose that it enters the silicon site. The substitution of lithium or magnesium by Cr^{IV} or Cr^{V} would require charge compensation therefore we propose that the second type of evidenced environment arises from a distorted site of Si rather than from a real substitution of Li or Mg. Another interpretation of this EXAFS result could be that even the single crystals of LMS are polluted at the grain boundaries or at the surface by $LiCrO_2$, since the second observed distance for chromium corresponds to that of chromium in $LiCrO_2$. In this case, the chromium in the parasitic phase would represent about 30% of the total chromium analysed, which means that $LiCrO_2$ should be present only as traces in these samples (since the total amount of chromium in sample B is only 0.03% wt.).

Conclusion

The investigations reported here for Cr:LMS clearly show that samples prepared by solid state reaction always contain a parasitic phase $LiCrO_2$ even at very low chromium content, hence the importance of single crystal elaboration. Diffuse reflectance studies on ground crystals obtained by flux method reveal that chromium is in three valence states. Results of the EXAFS study show that chromium is distributed between two types of environment which could reveal in fact the presence of $LiCrO_2$ as trace even in LMS crystals (surface or internal pollution). One location of the Cr (Cr–O = 1.68 Å) should correspond to the silicon site in LMS. Even if the actual amount of Cr^{IV} is low, its very high fluorescence lifetime value is demonstrated in Cr:LMS single crystals. Further investigations dealing with a more comprehensive study of EXAFS-XANES of chromium in crystals and *ab initio* calculations of Cr^{IV} energy levels in LMS lattice, are in progress.

References

1 V. Petricevic, S. K. Gayen, R. R. Alfano, K. Yamagishi, H. Anzai and Y. Yamaguchi, *Appl. Phys. Lett.*, 1988, **52**(13), 1040–1042.
2 V. Petricevic, S. K. Gayen and R. R. Alfano, *Appl. Phys. Lett.*, 1988, **53**(26), 2590–2592.
3 H. R. Verdun, L. M. Thomas, D. M. Andrauskas, T. McCollum and A. Pinto, *Appl. Phys. Lett.*, 1988, **53**(26), 2593–2595.
4 G. M. Zverev and A. V. Shestakov, in *OSA Proc. Tunable Solid State Lasers*, Springer-Verlag, 1989, **5**, 66.
5 W. Jia, H. Eilers, W. M. Dennis, W. M. Yen and A. V. Shestakov, *OSA Proceedings on Advanced Solid State Lasers*, Optical Society of America, Washington D.C., U.S.A., eds. L. Chase and A. Pinto, 1992, **13**, 31–33.
6 Y. P. Tong, P. M. W. French, J. R. Taylor and J. O. Fujimoto, *Opt. Commun.*, 1997, **136**(3–4), 235–238.
7 A. Seas, V. Petricevic and R. R. Alfano, *Opt. Lett.*, 1993, **18**, 891–893.
8 Y. P. Tong, T. M. Sutherland, P. M. W. French, T. R. Taylor, A. V. Shestakov and B. H. T. Chai, *Opt. Lett.*, 1996, **21**(9), 644–646.
9 B. Lipavsky, Y. Kalisky, Z. Burshtein, Y. Shimony and S. Rotman, *Opt. Mater.*, 1999, **13**(1), 117–127.
10 S. Kück, S. Hartung, K. Petermann and G. Huber, *Appl. Phys. B: Lasers Opt.*, 1995, **61**, 33–36.
11 D. E. Budil, D. G. Park, J. M. Burlitch, R. F. Geray, R. Dieckmann and J. H. Freed, *J. Chem. Phys.*, 1994, **101**(5), 3538–3548.
12 C. Anino, J. Théry and D. Vivien, *Opt. Mater.*, 1997, **8**, 121–128.
13 R. Moncorge and H. Manaa, *Ann. Chim. (Paris)*, 1995, **20**, 241–248.
14 A. R. West and F. P. Glasser, *J. Mater. Sci.*, 1971, **6**, 1100–1110.
15 H. Yamaguchi, *Yogyo Kyokaishi*, 1981, **89**(4), 203–208.
16 H. Yamaguschi, K. Akatsuka and M. Setoguchi, *Acta. Crystallogr., Sect. B Struct. Crystallogr. Cryst. Chem.*, 1979, **35**, 2678–2680.
17 H. Yamaguchi, K. Akatsuka, M. Setoguchi and Y. Takaki, *Acta. Crystallogr., Sect. B Struct. Crystallogr. Cryst. Chem.*, 1979, **35**, 2680–2682.
18 U. Hömmerich, H. Eilers, S. M. Jacobsen, W. M. Yen and W. Jia, *J. Lumin.*, 1993, **55**, 293–301.
19 K. Cerqua-Richardsen, B. Peng and T. Izumitani, in *OSA Proc. Advanced Solid State Lasers*, Optical Society of America, Washington D.C., U.S.A., eds. L. Chase and A. Pinto, 1992, **13**, 52.
20 E. Moya, C. Zaldo, B. Briat, V. Topa and F. J. Lopez, *J. Phys. Chem. Solids*, 1993, **54**(7), 809–816.
21 C. Simo, E. Banks and S. L. Holt, *Inorg. Chem*, 1970, **9**, 183.
22 J. B. Milstein, J. Ackerman, S. Holt and B. R. McGarvey, *Inorg. Chem.*, 1972, **11**, 1178.
23 V. F. Sears, in *Thermal neutron scattering lengths and cross sections for condensed matter research*, Chalk River Nuclear Lab., Internal Report AECL-8490, 1984.
24 R. D. Shannon, *Acta Crystallogr. Sect. A: Cryst. Phys., Diffr., Theor. Gen. Cryst.*, 1976, **32**, 75.
25 P. W. McMillan, *Glass-Ceramics*, 2nd edn., Academic Press, London, New-York, San Fransisco, 1979, p 80–82.
26 A. Michalowicz, *EXAFS pour le Mac, Logiciels pour la Chimie*, Société Française de Chimie, Paris, 1991, p. 102.
27 B. K. Teo, *EXAFS Basic Principles and Data Analysis*, Springer-Verlag, Berlin, 1986.
28 J. J. Rehr and R. C. Albers, *Rev. Mod. Phys.*, 2000, **72**, 621–654.
29 K. E. Miyano, J. C. Woicik, P. Sujatha Devi and D. Gafney, *Appl. Phys. Lett.*, 1997, **71**(9), 1168–1170.
30 J. J. Rehr and R. C. Albers, *Phys. Rev. B: Condens. Matter*, 1990, **41**, 8139.
31 J. Munstre de Leon, J. J. Rehr, S. I. Zabinsky and R. C. Albers, *Phys. Rev. B: Condens. Matter*, 1991, **44**, 4146.
32 S. J. Zabinsky, J. J. Rehr, A. Ankundinov, R. C. Albers and M. J. Eller, *Phys. Rev. B: Condens. Matter*, 1995, **52**, 2995.